# Multi-parameter FWI imaging in the Llanos Basin, onshore Colombia

*Mason Phillips*, James McLeman, Mike Varner, DUG Technology*
*Marco Perez and Doug Brost, Parex Resources*

**Summary**

Accurate seismic imaging in the vicinity of lateral velocity variations across fault planes is one of the many common challenges in the conventional seismic imaging workflow. Subvolumes of poor illumination, false structure, low resolution, and low amplitude are often observed in the footwalls of faults due to inaccurate velocity estimation and/or the use of ray-based imaging algorithms. This phenomenon is commonly called the "fault shadow" problem and typically relies on interpretation-driven scenario testing, which is labor-intensive and subjective. Multi-parameter full-waveform inversion (MP-FWI) imaging is an alternative to the conventional workflow that can be used to overcome fault shadow imaging challenges. In this study, we use MP-FWI imaging to simultaneously estimate a P-velocity (Vp) model and least-squares reflectivity image using partially pre-processed seismic data acquired in the Llanos Basin, onshore Colombia. This implementation of MP-FWI imaging improves the resolution of the Vp model and reflectivity image in fault shadow areas where interpretation-driven model-building workflows may fail.

**Introduction**

Conventional seismic imaging algorithms depend on a variety of assumptions, which may include ray-based, single-arrival, or Born approximations. Complex pre-processing workflows are therefore required to satisfy the assumptions of conventional imaging algorithms. MP-FWI imaging enables a simplified pre-processing workflow by using the full wavefield, including all orders of multiple reflections, in a more advanced imaging algorithm that does not depend on ray-based, single-arrival, or Born approximations that may be assumed in conventional imaging algorithms. This implementation of FWI separates the kinematics and dynamics of the wavefield to robustly perform a simultaneous inversion such that reflectivity, Vp, and other Earth parameters can be determined. The derived Vp model is suitable for conventional imaging, should it be required, and the reflectivity image is suitable for both structural interpretation and quantitative analysis (McLeman et al., 2022). Multi-parameter inversion challenges, such as crosstalk and relative scaling differences, are addressed through the use of a novel second-order quasi-Newton method (McLeman et al., 2023). The inclusion of multi-scattering events, together with the least-squares imaging approach, results in improved illumination and amplitude reconstruction, especially in areas with complex geology (Rayment et al., 2023; Phillips et al., 2024).

In sedimentary basins around the world, including the Llanos Basin, onshore Colombia, Vp variations across faults often lead to poor seismic imaging when using conventional methods. The resulting fault shadows increase uncertainties in the interpretation of potential reservoirs, which is critical for field development and/or prospect evaluation. Previous attempts to improve the imaging in fault shadows using more conventional methods, such as interpretation-driven scenario testing, fault-constrained reflection tomography, and ray-based migration, were beneficial but a higher-resolution solution was needed. In this paper, we demonstrate the successful application of the novel MP-FWI imaging approach outlined by McLeman et al. (2023) and Phillips et al. (2024) to further improve the imaging in areas previously obscured by fault shadows, using explosive source seismic data acquired in the Llanos Basin, onshore Colombia.

**Method**

The model-building workflow begins with first break picking and refraction tomography using the raw field data. The resulting refraction tomography Vp model was merged with a heavily smoothed legacy Vp model. The merge zone was defined based on a refraction illumination attribute computed using ray tracing.

Diving-wave FWI was then used to refine the near-surface Vp model. The only pre-processing applied to the input data was surface-consistent deconvolution estimated from the refracted arrivals to account for wavelet variability in the field data. The shot-consistent deconvolution operators effectively removed the source ghost, which varied spatially based on hole depth. After applying the surface-consistent deconvolution operators, the data was re-datumed to the surface with an uphole correction to avoid forward modeling the source ghost. Although the data quality supported starting diving-wave FWI at lower frequencies, forward modeling tests indicated no cycle skipping at 7 Hz, so diving-wave FWI started at 7 Hz and proceeded to 17 Hz in four frequency steps.

In parallel with near-surface Vp model building, we applied a pre-processing workflow that included iterative surface-consistent residual reflection static corrections, linear noise attenuation, surface-consistent deconvolution (using reflections), and random noise attenuation. The station spacings are sparse, the linear noise is generally

quite slow, and the data was acquired with geophone arrays. The geophone arrays partially attenuate the linear noise, but enhance the aliased portion of the noise, which makes the residual linear noise attenuation more challenging.

The data with the abbreviated pre-processing was then Kirchhoff prestack depth migrated using the refraction FWI Vp model merged with the smoothed legacy Vp model. Multiple reflections were removed with a mute in the parabolic Radon domain. These conditioned gathers were used to pick residual moveout curves and update the long-wavelength component of the deep Vp model using reflection tomography. The data was then re-migrated with the updated Vp model. Kinematic variations consistent with strong anisotropy were observed below the top of the Leon formation. Initial anisotropy models were built by integrating residual moveout picks with depth errors estimated from well markers. At this stage in the model-building workflow, the initial anisotropy models were constrained to be one-dimensional functions. Finally, one additional pass of TTI reflection tomography was performed to update the background Vp model before proceeding with MP-FWI imaging.

The previously described preprocessing workflow was extended to include surface-consistent scaling, residual dip filtering targeting relatively low-amplitude converted waves, and random noise attenuation. It is important to note that this abbreviated pre-processing workflow does not include any demultiple or 5D common offset vector tile (COV) interpolation/regularization, which are typically time-consuming and subjective steps in the conventional pre-processing workflow. A zero-phase statistical wavelet was estimated from the prestack data to be used for MP-FWI imaging. Gardner's equation (Gardner et al., 1972) was used to derive the initial density model from the Vp model, then heavily smoothed (2 km vertical x 10 km horizontal) to retain only the long-wavelength trend. A constant or smooth well-based starting density model would have also been equally effective. For all inversions, we assumed uniform anelastic attenuation with Q = 100.

The viscoacoustic MP-FWI imaging stage of the workflow started at 17 Hz and proceeded to 38 Hz in four frequency steps. All inversions used all shots and output an updated Vp and reflectivity simultaneously.

**Results**

Diving-wave FWI successfully increased the resolution of the near-surface model, but the maximum magnitude of the Vp perturbation was only a few percent (Figure 4). We attribute the relatively small magnitude of the perturbation mainly to the accuracy of the refraction tomography Vp model, as evidenced by our ability to start diving-wave FWI at a relatively high frequency with no cycle skipping.

Viscoacoustic MP-FWI imaging was used to simultaneously determine an updated Vp model and reflectivity image. At each frequency, the Vp and reflectivity image resolution increased. At approximately 20 Hz, the alternating sand and shale layers in the Carbonera group began to be resolved (Figures 4 and 5). The Vp model output from each MP-FWI imaging frequency step was used as input to a Kirchhoff prestack depth migration (KDM) to validate the kinematic fidelity (Figure 2).

Before concluding the MP-FWI imaging workflow, the anisotropy parameters were updated using well marker misties. This update sharpens the boundaries of the thick, highly anisotropic shale layer between the tops of the Leon and Carbonera formations, and replaces a thick layer of weak anisotropy in the underlying Carbonera formation with thinner alternating layers of high and low anisotropy corresponding to the alternating shale and sand layers.

After finalizing the Vp model using MP-FWI imaging and calibrating the anisotropy models using the wells, some residual kinematic variations exist in the observed data that are not observed in the forward modeled data. To partially account for residual kinematic variations associated with unresolved small-scale anomalies in the near-surface, surface-consistent corrections were estimated and applied using the forward modeled data as a pilot. To take advantage of these corrections, they are applied to the observed data before an additional pass of FWI imaging, determining an updated reflectivity only. This is a novel approach for estimating surface-consistent residual static corrections specifically tailored for FWI.

The dynamic and kinematic match between the observed data and synthetic data forward modeled using the final Vp, density, and anisotropy models indicates the models estimated using MP-FWI imaging explain both the amplitude and phase of the data (Figure 1). To evaluate the MP-FWI imaging outputs, the fully pre-processed data was migrated using KDM and reverse-time migration (RTM) using the MP-FWI imaging Vp model. The KDM gathers migrated with the MP-FWI imaging Vp model are flatter than the KDM image gathers migrated with the initial MP-FWI imaging Vp model, derived using diving-wave FWI and reflection tomography (Figure 2). The MP-FWI image is generally higher resolution than the RTM and lowpass filtered KDM, and has a more uniform amplitude profile due to more robust illumination compensation (Figure 5). The yellow arrows in Figure 5 highlight areas with increased vertical and lateral resolution in the vicinity of complex faulting. The improved lateral resolution is

further demonstrated by computing the incoherence attribute, which emphasizes the seismic expression of discontinuous geological features, such as faults, channels, unconformities, and subtle stratigraphic features. The incoherence attribute computed using the MP-FWI image has higher resolution than the incoherence attribute computed using the legacy KDM, which was produced using a more laborious and subjective interpretation-driven model-building workflow (Figure 3).

**Conclusions**

We have demonstrated a successful application of MP-FWI imaging on land seismic data acquired in the Llanos Basin, onshore Colombia. The MP-FWI imaging reflectivity, using partially pre-processed data, shows an uplift compared to an RTM using the fully pre-processed data, particularly in the vicinity of faults. The improved kinematic accuracy of the MP-FWI imaging Vp model relative to the Vp model derived using diving-wave FWI and reflection tomography is further substantiated by favorable KDM comparisons using the fully processed seismic data.

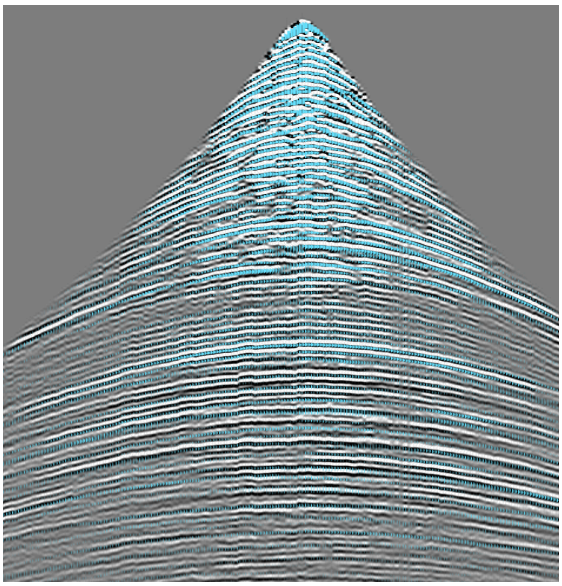

Figure 1: 38 Hz lowpass filter observed data (grayscale) with synthetic data forward modeled with the MP-FWI imaging Vp model overlaid (blue).

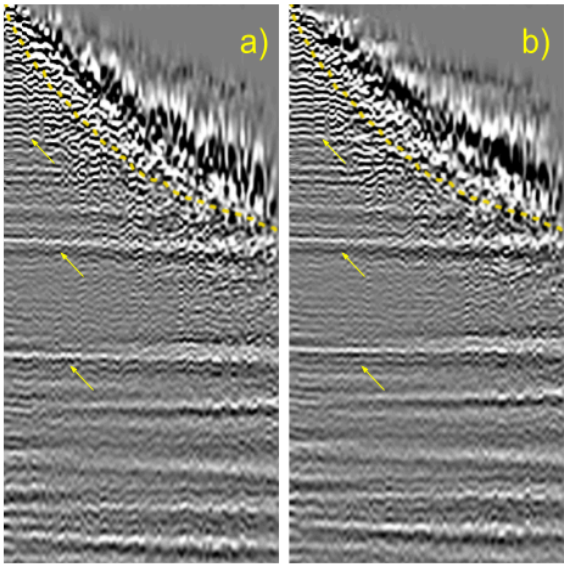


Figure 2: COV tile KDM gathers migrated with the (a) initial MP-FWI imaging Vp model (after diving-wave FWI and reflection tomography), and (b) the final MP-FWI imaging Vp model. The yellow arrows highlight areas of improvement after updating the Vp model using MP-FWI imaging. The yellow dotted line is a 50 degree angle mute.

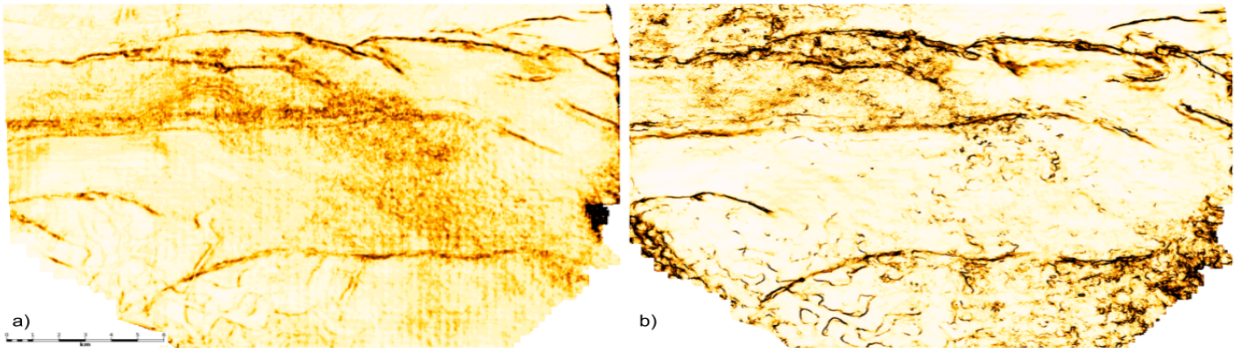


Figure 3: Incoherence depth slices estimated using a (a) legacy (2023) KDM stack and (b) 38 Hz MP-FWI reflectivity image.

## Llanos Basin MP-FWI imaging

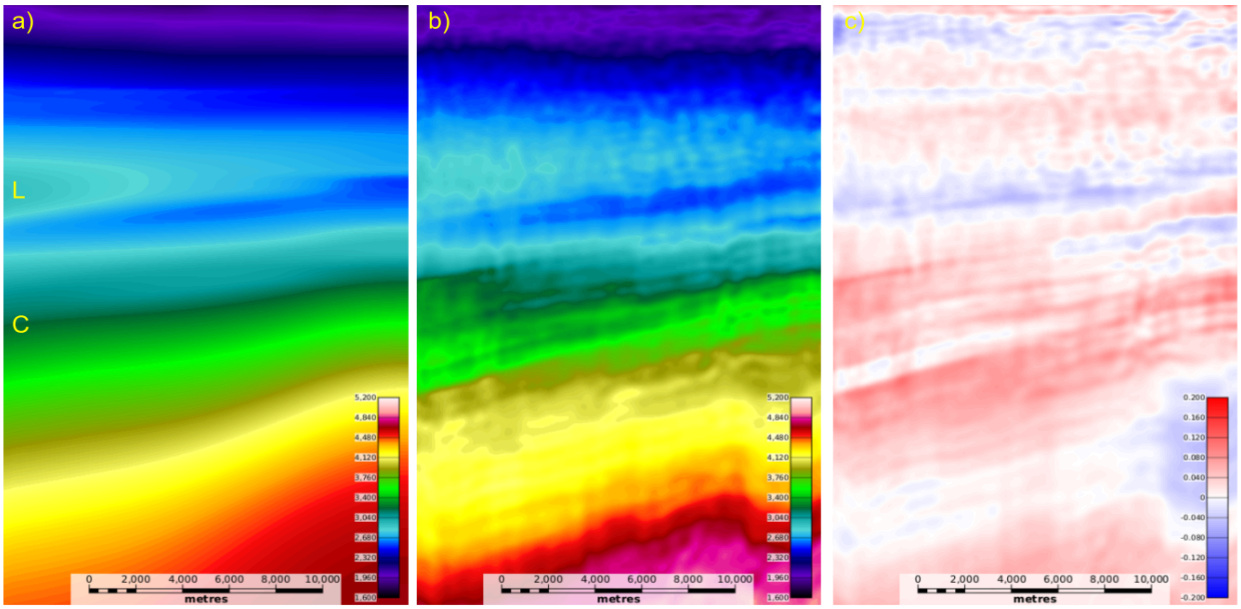


Figure 4: (a) Initial Vp model derived by merging refraction tomography Vp model and a heavily smoothed legacy Vp model, (b) 38 Hz MP-FWI imaging Vp model, and (c) total fractional velocity perturbation. On the left panel, the "L" corresponds to the approximate top of the Leon formation, and the "C" corresponds to the Carbonera group.

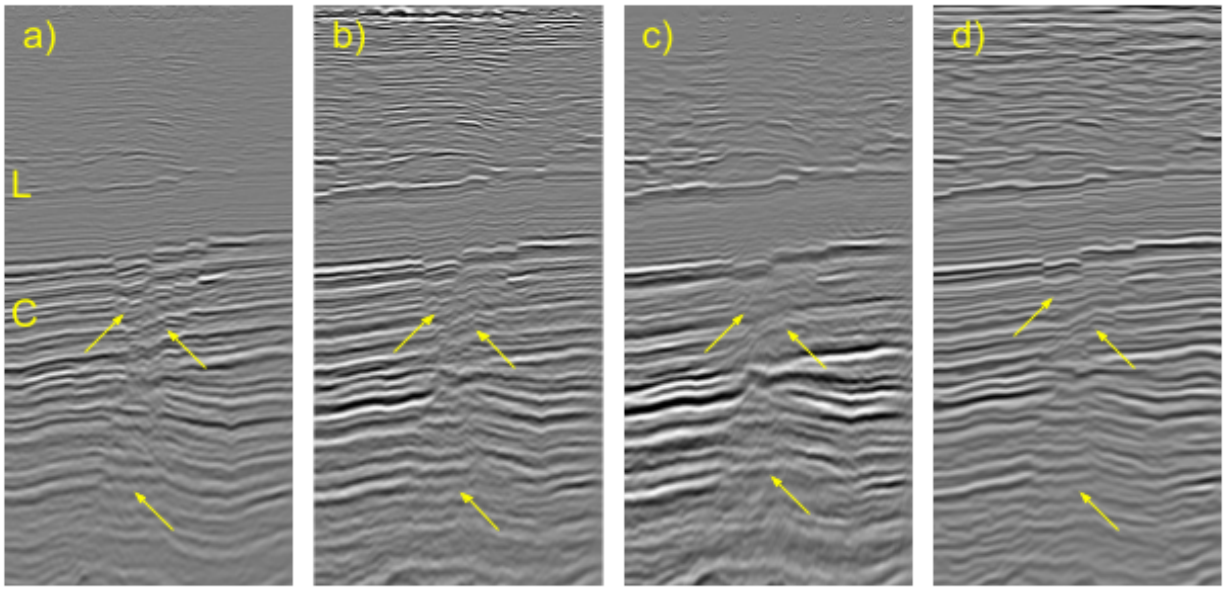


Figure 5: (a) 38 Hz lowpass filtered legacy (2023) KDM stack, (b) 38 Hz lowpass filtered KDM stack migrated with the MP-FWI imaging Vp model, (c) 38 Hz RTM migrated with the MP-FWI imaging Vp model, and (d) 38 Hz MP-FWI imaging reflectivity. On the left panel, the "L" corresponds to the approximate top of the Leon formation, and the "C" corresponds to the Carbonera group.